CrystEngComm

Accepted Manuscript

ROYAL SOCIETY OF CHEMISTRY

www.rsc.org/crystengcomm

Pr Nathalie Steunou

Institut Lavoisier (UMR CNRS 8180)

Université de Versailles-Saint-Quentin-en-Yvelines (UVSQ)

45 avenue des Etats Unis 78035 Versailles cedex

FRANCE

Tel : 33 1 39 25 43 73

Fax: 33 1 39 25 44 52

e-mail :nathalie.steunou@uvsq.fr

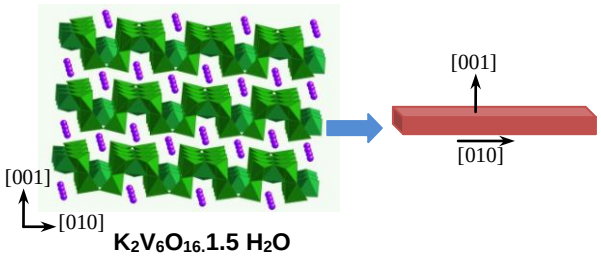

This highlight deals with the recent advances on the synthesis in aqueous solution of one-dimensional vanadium (V) oxide nanocrystals.

Table of contents entry

Steunou et al

Rational design of one-dimensional vanadium(V) oxide nanocrystals: an insight into the physico-chemical parameters controlling the crystal structure, morphology and size of particles.

Nathalie Steunou.[*,a] Jacques Livage,[bcd]

In this highlight, we cover the recent advances on the different synthetic strategies in aqueous solution of one-dimensional vanadium (V) oxide nanocrystals including nanowires, nanotubes, nanorods, nanobelts and nanorings. We have focused mainly our attention on nanostructured materials based on V_2O_5, $M_xV_2O_5$ (M= Li, Ag, Na…), MV_3O_8 and $M_2V_6O_{16}$ (M = Li, Na, NH_4, K…) phases that are currently investigated as cathodes for Li-ion batteries. Here, this article intends to provide a comprehensive review of the synthesis of vanadium oxide nanostructures by combining sol-gel chemistry and hydrothermal processes with the aim of mastering the nanostructure formation and elucidating the fundamental processes of crystallization. Therefore, our discussion has been mainly focused on the identification of the synthetic parameters that drive the structure, crystallinity, size and morphology of nanocrystals. In some cases, possible mechanisms for the nucleation and growth of vanadium oxide nanocrystals were proposed.

1. Introduction

In the past decades a remarkable progress has been realized in the synthesis of nanomaterials differing in microstructure, texture and chemical composition. The

[a] *Institut Lavoisier de Versailles, UMR CNRS 8180, UVSQ, 45 avenue des Etats-Unis 78035 Versailles Cedex. France. E-mail: nathalie.steunou@uvsq.fr Fax: +33 1 39 25 43 73 ; Tel : +33 1 39 25 44 52.*
[b] *Sorbonne Universités, UPMC Univ Paris 06, UMR 7574, Chimie de la Matière Condensée de Paris, F-75005, Paris, France,*
[c] *CNRS, UMR 7574, Chimie de la Matière Condensée de Paris, F-75005, Paris, France.*
[d] *Collège de France, UMR 7574, Chimie de la Matière Condensée de Paris, F-75005, Paris, France.*

development of these nanostructured materials has become an extensive challenge since their fascinating physical properties can be tuned by tailoring the size, morphology, crystallinity and surface functionality of nanocrystals, opening up new perspectives in the development of nanodevices.[1] Moreover, due to ecological concerns, it is of primary importance to significantly reduce the necessary amount of functional materials and process them with a "green technology" using low-cost and environmentally friendly synthesis procedures (precursors and solvent of low toxicity).[2] The emerging energy resource crisis and the environmental issues have stimulated the exploration and development of renewable energy technologies, including better energy storage technologies that are required for the development of portable power supplies or the next generation of automobiles.[3,4] Li-ion batteries have achieved significant progress in energy storage performance despite of the fact that the increase of their energy density is often limited by the Li^+ intercalation capacity of the cathode.[3,5,6,7] Therefore, the engineering of nanostructured electrode materials has been reported in the past few years and the enhanced energy storage properties of these electrodes are attributed to faster kinetics of Li^+ diffusion, higher capacity and better cyclic stability.[3-6]

Reported initially by Whittingham a few decades ago,[8] V_2O_5 has been extensively investigated for Li-batteries because of its high abundance, low cost, its layered crystal structure accessible for ion intercalation and high theoretical capacity (about 294 mAh g^{-1} with 2 Li insertion per unit formula).[3-9] However, the intrinsic low diffusion coefficient of Li^+ ($D \sim 10^{-12}$ cm^2 s^{-1}) and poor electronic conductivity (10^{-2} to 10^{-3} S cm^{-1}) in crystalline V_2O_5 largely limits the practical application of this cathode material. In order to circumvent these difficulties, numerous low-dimensional nanostructured vanadium oxides (i. e. nanowires, nanorods, nanotubes, nanobelts, nanosheets) have been reported since their enhanced capacity and cyclic stability arise from their large interfacial contact area with the electrolyte, the short Li-ions transport distance, 1D electron transport pathways and facile strain relaxation upon

electrochemical cycling.[3,6,7,10] This strategy has been applied to numerous nanostructured vanadium oxides including mainly V_2O_5,[11,12,13] $M_xV_2O_5$ (M= Li, Ag, Na…),[14,15,16,17] MV_3O_8 or $M_2V_6O_{16}$ (M = Li, Na, NH_4, K…),[18,19] VO_x nanotubes[20] and $Ag_2V_4O_{11}$.[21] The strong interest in the exploration of vanadium oxide nanostructures has led to the exploration of numerous synthetic strategies including reverse-micelle synthesis,[11] sol-gel and hydrothermal processes,[14-19] template-assisted electrodeposition,[7,22] electrospinning,[23] thermal evaporation method,[24] and microwave.[25] However, the possibility of controlling the nanocrystal morphology, structure and defects still remains a challenge and the practical application of these materials is often limited by the absence of controllable and repeatable synthetic pathways. Therefore, the possibility of mastering the synthesis of nanostructured materials with monodisperse morphology is the key to achieving reproducible samples and is also crucial for the scaling-up of laboratory syntheses into reliable manufacturing procedures.

The present article is intended to give a useful survey of recent progress in the synthesis of one-dimensional vanadium oxides including V_2O_5, $M_xV_2O_5$ and MV_3O_8 (or $M_2V_6O_{16}$). This paper is focused on the most commonly used sol-gel (in aqueous solution) and hydrothermal procedures. The sol-gel routes based on vanadium alkoxides are not considered due to the high reactivity of these precursors towards moisture which limits the large-scale production of nanomaterials. Review on the synthesis of V_2O_5 nanostructures by template and template-based electrodeposition processes can be found in Wang's article.[7] Our interest devoted to the synthesis routes in solution is related to the possibility of addressing the influence of a few physico-chemical parameters (pH, concentration, precursors, temperature, ionic strength…) on the composition, crystallinity and morphology of nanocrystals. Moreover, in some peculiar cases, some reactional intermediates can be identified by sampling and characterizing the reaction medium (supernatant solution and solids) by in-situ or ex-situ methods at different

times. This strategy may shed light on the nucleation and growth mechanism of nanostructured vanadium oxides which is of primary importance to master their production.

2. Sol-gel synthesis of $V_2O_5.nH_2O$ gels, $M_xV_2O_5.nH_2O$ intercalates, $MV_3O_8.nH_2O$ and $M_xV_6O_{16}.nH_2O$

The synthesis of 1D nanostructured vanadium oxides in solution is based on the sol-gel synthesis of vanadium oxides. This part summarizes the fundamental knowledge collected these past few years concerning the reactivity of V(V) in aqueous solution and its polymerization into $V_2O_5.nH_2O$, $MV_3O_8.nH_2O$ and $M_xV_6O_{16}.nH_2O$ phases. A formation mechanism of these oxides was proposed.

2.1 Polymerization of V(V) in aqueous solution: synthesis of $V_2O_5.nH_2O$ gels

It is well known that that a large variety of oxo-anions of V(V) exist in aqueous solution, depending on pH and vanadium concentration (see Fig. 1). V(V) is six fold coordinated at acidic pH and four-fold coordinated at basic pH. At pH> 14, $[VO_4]^{3-}$ (orthovanadate) is the main vanadate present in solution and upon decreasing pH, protonation occurs giving rise to monomeric hydrolysed vanadates at low concentration (i. e. $[H_nVO_4]^{3-n}$) or oligomeric vanadates ($[V_2O_7]^{4-}$ (pyrovanadate), $[V_4O_{12}]^{4-}$ (metavanadate), $[H_nV_{10}O_{28}]^{6-n}$ (decavanadates)). These oligomeric vanadates are formed by condensation reactions of $[HVO_4]^{2-}$:[26]

Oxolation: V-OH + V-OH = V-O-V + H_2O (1)

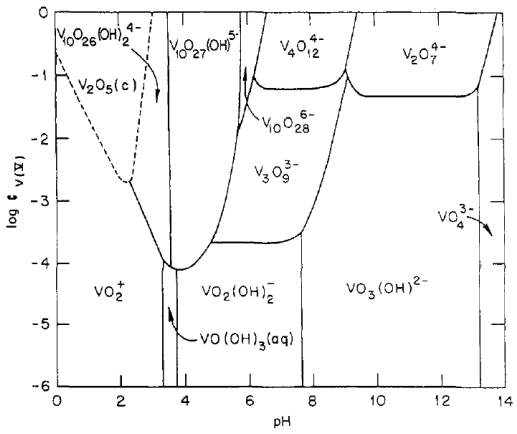

Fig. 1 Predominant V(V) oxo species in aqueous solution at 25°C as a function of vanadium concentration C and pH. Reprinted with permission from J. Livage, *Chem. Mater.*, 1991, **3**, 578.[27] Copyright (1991) American Chemical Society.

As previously reported, $V_2O_5.nH_2O$ gels can be obtained from aqueous solutions around pH ~ 1.5. The structure of $V_2O_5.1.8\ H_2O$ xerogels resolved by Petkov *et al*[28] using the atomic pair distribution function (PDF) technique, can be described as an assembly of V_2O_5 bilayers made of square pyramidal VO_5 whose interlayer space is occupied by water molecules (Fig. 2(a)). These hydrated vanadium oxides are found as stacked ribbon-like particles about 10-20 nm wide and a few µm long as shown in the TEM image of Fig. 2(b). More details concerning the synthesis, structure and electronic properties of $V_2O_5.nH_2O$ gels are provided in the review of J. Livage.[27] The $V_2O_5.n\ H_2O$ gels can be prepared through different methods of acidification of metavanadates including the addition of mineral acid or the use of a proton exchange resin. However, since $V_2O_5.nH_2O$ gels are generally obtained at low ionic strength, the acidification method with a proton exchange resin is particularly efficient and classically used for their preparation. A metavanadate solution is passed through the resin and a pale yellow solution of decavanadates is first formed. Upon elution of the vanadate solution, an orange solution with a high concentration of decavanadates is formed that spontaneously polymerizes into vanadium (V) oxo-polymers. The solution becomes more viscous and gelation occurs within a few hours for a vanadium concentration higher than 0.1 mol. L^{-1}. A dark red gel is obtained which consists of highly condensed ribbon-like particles (Fig. 2(b))

entrapped in a solution of $[H_nV_{10}O_{28}]^{(6-n)-}$ and cationic $[VO_2]^+$ species. ^{51}V NMR spectra were recorded on acidic vanadate solution obtained with the proton exchange resin, showing that this solution contains a mixture of anionic $[H_2V_{10}O_{28}]^{4-}$ ($\delta(^{51}V)$ = -420, -512, -530 ppm) and cationic $[VO_2]^+$ species ($\delta(^{51}V)$ = -545 ppm) which can serve as a reservoir for V(V) precursors.[29] The pH of the solution increases slightly, from 1 to 1.5, during the formation of the gel. This may be due to the protonation of $[H_2V_{10}O_{28}]^{4-}$ decavanadate species in order to provide zero-charge precursors (eq 1).[26,29]

$$[H_2V_{10}O_{28}]^{4-} + 4\ H^+ + 32\ H_2O = 10\ [VO(OH)_3(H_2O)_2] \quad (1)$$

The V_2O_5 network present may be formed via the polycondensation of the neutral precursor $[VO(OH)_3(OH_2)_2]^0$ through oxolation (1) and olation (2) reactions.[26,27] The olation reaction can be written as follows:

$$\textit{Olation}: \text{V-OH} + \text{V-}\ H_2O = \text{V-OH-V} + H_2O \quad (2)$$

One main disadvantage of using a proton exchange resin is the difficulty to control the vanadium concentration which varies from the beginning of the exchange process to the end. Moreover, some foreign ions such as Na^+ may be present and remain in the gel even after ion exchange. This is the reason why $V_2O_5.nH_2O$ gels are also commonly prepared by the dissolution of crystalline V_2O_5 in a solution of hydrogen peroxide.[30] This reaction gives rise to an orange solution containing the diperoxo V(V) complex (i. e. $[VO(O_2)_2]^-$) as clearly evidenced by ^{51}V NMR spectroscopy ($(\delta(^{51}V)$ = -695 ppm).[30] These complexes are unstable and the progressive oxidation of H_2O_2 in excess and peroxo ligands into oxygen gas occurs. A very acidic solution of pH 1.5 is then formed after 2h that contains the monoperoxo V(V) complex (i. e. $[VO(O_2)]^+$) and polyoxovanadates species (i. e. $[H_2V_{10}O_{28}]^{4-}$ and $[VO_2]^+$) identified by ^{51}V NMR in solution ($\delta(^{51}V)$ = -539 ppm for $[VO(O_2)]^+$).[30] After 3 h, only $[H_2V_{10}O_{28}]^{4-}$ and $[VO_2]^+$ are detected in solution by ^{51}V NMR which means that a similar acidic vanadate solution is obtained by this method compared to that of obtained through a

proton exchange resin. This solution progressively polymerizes and a dark red gel is obtained after about 24 h.

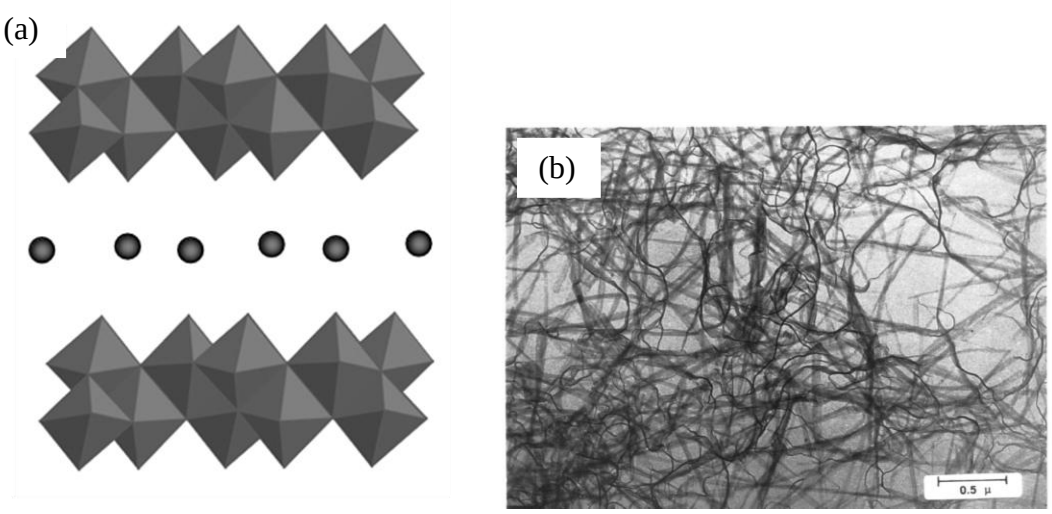

Fig. 2 (a) Projection of the structure of V_2O_5. $1.8H_2O$ along [010],[29] (b) TEM image of $V_2O_5.nH_2O$ gels. For (b), reprinted with permission from J. Livage, *Chem. Mater.*, 1991, **3**, 578.[27] Copyright (1991) American Chemical Society.

2.2 Intercalation of cations in $V_2O_5.nH_2O$ gels: formation of $M_xV_2O_5$ intercalates.

It is known that the ribbon-like particles of $V_2O_5.nH_2O$ are negatively charged and exhibit acid properties (0.3-0.4 H^+ per V_2O_5).[27,29] This can be explained by the strong polarizing power of the V^{5+} cation which leads to an acidic dissociation of V-OH groups at the oxide-water interface. Therefore, it is possible to incorporate cations between the layers of the gels and this process involves ion-exchange reactions with the acid protons of the gels. Therefore, the exchange capacity, i.e. the cation content M/V_2O_5 ($x \sim 0.3$ for M^+ and $x \sim 0.15$ for M^{2+}) corresponds to the amount 0.3-0.4 H^+/V_2O_5.[27,29] This intercalation process can be performed after the gel preparation (by dipping a V_2O_5 gel in a solution of ionic salts)[31] or during the course of V(V) polymerization.[29] Moreover, the $V_2O_5.1.8H_2O$ xerogel can serve as a host matrix for the intercalation of a wide range of chemical entities including cations and organic molecules.[32] In the case of molecular species, it has been reported that the intercalation

proceeds through proton-transfer reactions with the protons of the gel, redox reactions or dipolar adsorption.[27]

2.3 Influence of pH and the nature of cations on the crystallization of MV_3O_8 and $M_xV_6O_{16}$.

$V_2O_5.nH_2O$ gels and $M_xV_2O_5.nH_2O$ intercalates are formed in a very acidic vanadate solution (pH~1 to 1.5). However, by increasing pH, $MV_3O_8.nH_2O$ and $M_xV_6O_{16}.nH_2O$ (x=1 for M^{II} and x=2 for M^{I}) precipitates can be obtained. These solids can be prepared by adding a small amount of base to the acidic vanadate solution obtained with the proton exchange resin. As an example, $NaV_3O_8.1.5H_2O$ can be obtained in a narrow range of pH, typically between 2 and 5.[29] Fig. 3 shows the X-ray diffraction patterns of the solids precipitated with an initial pH_i of 2.0 after various ageing times. It is worth noting that the intensity of the peaks corresponding to the hydrated vanadium oxide phase $Na_{0.3}V_2O_5.1.5H_2O$ decreases progressively while new peaks begin to appear. This new diffraction pattern corresponds to the low temperature

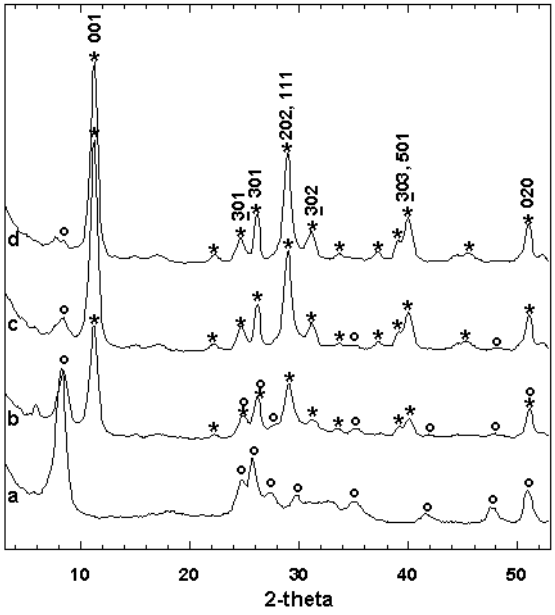

Fig. 3 X-ray diffraction patterns of solids synthesized in solution at pH_i=2.0 and left at 40°C for different ageing times (a) 2 days, (b) 6 days, (c) 13 days (d) 20 days. $Na_{0.3}V_2O_5.1.5H_2O$ peaks are represented by (°) ; $NaV_3O_8.1.5H_2O$ peaks are represented by (*).[29]

sodium trivanadate phase $NaV_3O_8.1.5H_2O$ already described in the literature.[33] Such progressive transformation and this precipitation of tri- or hexavanadates (i. e. $MV_3O_8.nH_2O$ and $M_xV_6O_{16}.nH_2O$ (x=1 for M^{II} and x=2 for M^{I})) at pH>1 were evidenced for a wide range of cations including monovalent (Li^+, Na^+, K^+, Cs^+, NH_4^+) and bivalent (Ca^{2+}, Mg^{2+} and Ba^{2+}) ones.[34,35] Tri- and hexavanadates obtained with Na^+, Mg^{2+}, Ca^{2+} and Ba^{2+} ions are isostructural and this framework can be described as a hewettite type structure (Fig. 4(a)) which is made up of layers with VO_5 trigonal bipyramid chains and distorted VO_6 octahedral chains sharing corners.[33,36] Tri- and hexavanadates with K^+, Cs^+ and NH_4^+ ions exhibit a different vanadium-oxide framework (Fig. 4(b)) made of twisted zigzag chains composed of VO_5 square pyramids sharing corners and edges and distorted VO_6 octahedra.[37] In both structures, cations are intercalated between the layers. The tri- or hexavanadate phase of a specific cation (Cs^+, NH_4^+ and Ba^{2+}) may present various amounts of intercalation water depending on initial pH conditions.

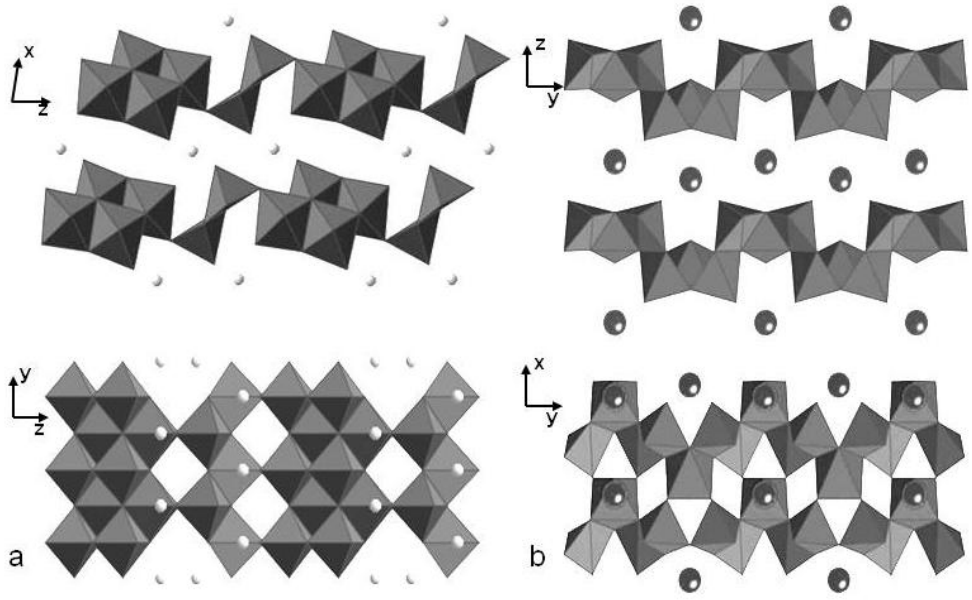

Fig. 4 (a) Projection of the structure of $Na[V_3O_8].1.5H_2O$ along [010] and [100]. (b) Projection of the structure of $Cs[V_3O_8]$ along [100] and [001]. Interlayer cations are represented as white (Na^+) and grey (Cs^+) circles.[35]

Depending on the nature of cation, tri- and hexavanadate phases precipitate directly from the vanadate solution or results from the progressive transformation of $M^{I}_{0.3}V_2O_5$ (or $M^{II}_{0.15}V_2O_5$) intercalates.[29,35] In the first case, they are formed in a short time (1 day) and at very acidic pH (pH 1-2) while in the second case, their formation occurs after at least 4 days and at higher pH (3-4). The kinetic of formation and thermodynamic stability of these phases seems to be strongly related to the nature of interlayer cations.[35] Depending on ionic radius of interlayer cations, three behaviours can be distinguished. For small cations like Mg^{2+}, Na^{+}, Ca^{2+} (r_{ion} < 1Å), tri- or hexavanadates are formed after at least 4 days at pH 3-4 while for larger cations like K^{+} and NH_4^{+} (1 <r_{ion} < 1.5Å), these oxides are obtained immediately after one day in the pH range 2-4.[35] Finally for large cations such as Cs^{+}, TMA^{+}, Ba^{2+} (r_{ion} > 1.35 Å), a competition is clearly observed between the formation of MV_3O_8 (or $M_xV_6O_{16}$) and that of the decavanadate polyanion.[35] The kinetics of tri- and hexavanadates formation is particularly low in pH conditions (typically in the range of pH 3-4) at which decavanadates are the most abundant vanadates in solution. As an example, CsV_3O_8 is obtained after one day at pH 1 and $Cs_2V_6O_{16}$.0.7 H_2O after 21 days at pH 3.[34] For 3<pH<4, $Cs_4[H_2V_{10}O_{28}].4H_2O$ has been isolated. It seems that the kinetics of the MV_3O_8 (or $M_xV_6O_{16}$) formation is related to the crystallographic structure of the tri- and hexavanadate phases. Indeed, the formation of tri- and hexavanadates phases with the hewettite structural type (Li^{+}, Na^{+}, Ca^{2+}, Mg^{2+}) is systematically delayed compared to that of vanadates with the $K_2V_6O_{16}$ type structure (K^{+}, Cs^{+}, NH_4^{+}).[35]

(a)

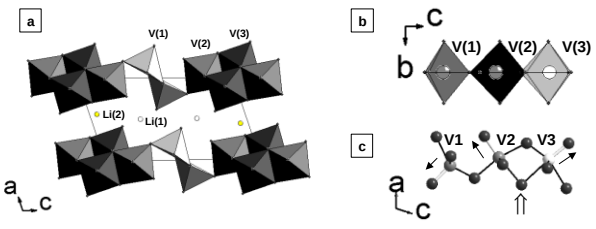

(b)

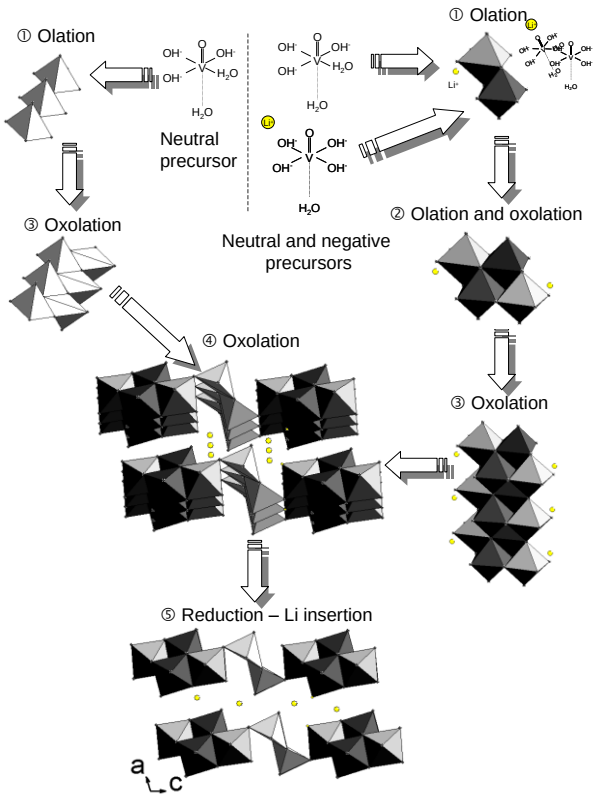

Fig. 5 (a) View of the $Li_{1+\alpha}V_3O_8$ structure along [010] and the three vanadium sites along [100] and [010]. (b) Proposed mechanism for the formation of $Li_{1+\alpha}V_3O_8$. Reprinted with permission from M. Dubarry, J. Gaubicher, D. Guyomard, O. Durupthy, N. Steunou, J. Livage, N. Dupré, C. P. Grey. *Chem. Mater.*, 2005**, 17**, 2276 Copyright (2005) American Chemical Society.[38]

Besides, since neither the $M_xV_2O_5$ nor the decavanadate polyanion present a structural relationship with the MV_3O_8 (or $M_xV_6O_{16}$) structures, the formation of these vanadium oxides implies certainly a redissolution-precipitation process. Since the composition of the V(V) solution changes with increasing pH, a vanadate solution of pH > 1 presumably contains a mixture of a neutral species $[VO(OH)_3(OH_2)_2]^0$ and a negatively charged precursor $[VO(OH)_4(OH_2)]^-$ as previously reported.[29] According to the so-called partial charge model,[39] it was possible to calculate that a solution at a pH = 4.5 corresponds to a mixture of $[VO(OH)_3(OH_2)_2]^0$ and $[VO(OH)_4(OH_2)]^-$ in the ratio 2:1.[29] A possible mechanism for the formation of $Li_{1+\alpha}V_3O_8$ that involves the condensation of both $[VO(OH)_3(OH_2)_2]^0$ and $[VO(OH)_4(OH_2)]^-$ has been proposed (see Fig. 5).[38] Three vanadium sites (noted V(1), V(2),

and V(3)) and two lithium sites (noted Li(1) and Li(2)) are present in the structure of $Li_{1+\alpha}V_3O_8$. The double chain related to V(1) (square-pyramid site) is similar to that in the structure of $V_2O_5.nH_2O$ gel, whereas the quadruple chain (V(2)-V(3)) (octahedral site) and particularly the orientation of vanadyl bonds (V=O) are characteristic of $Li_{1+\alpha}V_3O_8$. Due to the presence of these two types of V chains, two groups of condensation reactions were considered whether they lead to double chains of V(1) or quadruple chains of V(2)-V(3). This mechanism has been divided into five steps, as summarized in Figure 5(b).[38] The first group of reactions involves one of the two neutral precursors and gives rise to double chains of V(1) upon olation (step 1, left) and oxolation (step 2, left) reactions, as for V_2O_5. In the second group, one neutral and one negatively charged precursor can form edge-sharing dimers via an olation reaction (step 1, right) and Li^+ may have an influence on the orientation of the two precursors. Tetramers would be formed (step 2, right) via olation and oxolation reactions leading finally to a quadruple chain of octahedra by oxolation (step 3, right). The as-formed quadruple chain corresponds to the V(2)-V(3) chains found in the structure of $Li_{1+\alpha}V_3O_8$. At this point, a double chain V(1) and a quadruple chain V(2)-V(3) are formed and can condense via a last oxolation reaction (step 4) leading to $Li_{1+\alpha}V_3O_8$.

3. Hydrothermal synthesis of 1D nanostructured V_2O_5, MV_3O_8 and $M_2V_6O_{16}$

3.1 Anisotropic growth of micro- and nanocrystals of $V_2O_5.nH_2O$, MV_3O_8 and $M_2V_6O_{16}$.

As previously reported, the sol-gel synthesis of $V_2O_5.nH_2O$, MV_3O_8 and $M_2V_6O_{16}$ at room temperature lead to the formation of quite large 1D (nanorod, fibers, …) and 2D (platelets,…) crystallites whose dimension ranges generally between hundreds nanometres and a few micrometres. Most precipitates of MV_3O_8 and $M_xV_6O_{16}$ (x=1 for M^{2+} with $M^{2+} = Ca^{2+}$, Mg^{2+},

Ba^{2+} and x=2 for M^+ with M^+= Li^+, Na^+, K^+, Cs^+, NH_4^+) consist of rods (Fig. 6(c)-(d)), which are about 500 nm wide and a few micrometres long (see Fig. 6).

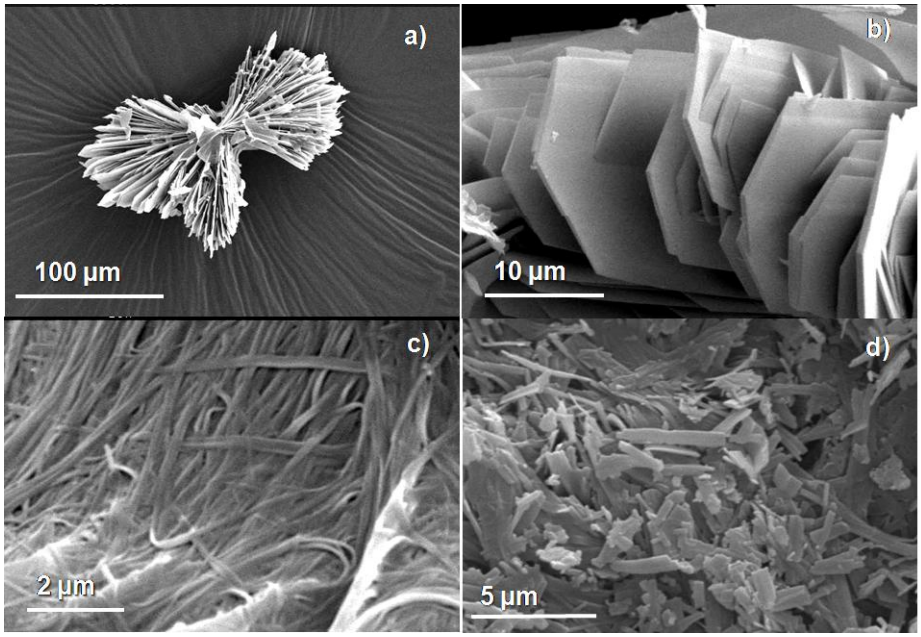

Fig. 6. SEM images of (a) and (b) $(NH_4)_2[V_6O_{16}].H_2O$ (pH_i=2; ageing time = 4 days) (c) $(NH_4)_2[V_6O_{16}].1.5H_2O$ (pH_i=3; ageing time = 14 days) (d) $K_2[V_6O_{16}].nH_2O$ (n=1.5 and 2.7) at pH 3.[35]

However, for the same cation, variation of the hydration rate of the vanadium oxide can strongly influence the particle morphology. As an example, for $(NH_4)_2[V_6O_{16}].H_2O$, one can observe by SEM butterfly like aggregates consisting of elongated platelet crystals which are hundreds µm long and 20 µm wide (Fig. 6). In contrast, the sample of $(NH_4)_2[V_6O_{16}].1.5H_2O$ is composed of entangled fibres of 10 µm long and 200 nm wide.[35]

Under hydrothermal conditions, nanocrystals of vanadium were obtained and four different nanostructure morphologies can be distinguished (Fig. 7). Monocrystalline or polycrystalline nanowires of V_2O_5, $(NH_4)_{0.5}V_2O_5$, $H_2V_3O_8$, $M_{0.33}V_2O_5$ (M=Ag, Na) and $Na_2V_6O_{16}.3H_2O$ with a diameter between 20 and 120 nm were synthesized.[15,18,40,41,42] Among the different vanadium oxides, the length varies significantly from a few 10 µm (i. e. $Na_2V_6O_{16}.3H_2O$[18] or $M_{0.33}V_2O_5$ (M=Ag, Na)[15]) to a few centimetres (i. e. V_2O_5).[42] Compared to nanowires, the aspect ratio of nanorods is notably lower. Nanorods of V_2O_5 and β-$Li_xV_2O_5$ which are about

tens nm wide and a few μm long were prepared.[17,43] Finally, nanobelts which can be described as single crystal nanowires with a rectangular cross-section were reported for numerous vanadium oxides including V_2O_5, $Na_{0.33}V_2O_5$, $(NH_4)_{0.5}V_2O_5$, $H_2V_3O_8$, $Na_{1.1}V_3O_{7.9}$, $NH_4V_3O_8$, $Ag_{1.2}V_3O_8$, $M_2V_6O_{16}$ (M= Na^+, K^+) and VO_x.[12,14,16,19,44,45,46,47,48,49,50,51] Their width typically varies between 20 and 500 nm and their length between tens and hundreds of micrometres. The anisotropy of the crystallite morphology can be related to the crystalline structure of vanadium (V) oxides. Actually in vanadium (V) oxides, the coordination sphere of V(V) is highly distorted due to the presence of a vanadyl bond V=O (d(V-O) ~ 1.55-1.75 Å) which is quite short in comparison to other V-O bonds (typically 1.9-2.0 Å). The *d-p* interaction of V and O in this double bond is responsible of a *trans-effect* which disfavours the bonding of a ligand in trans position of this vanadyl bond (d(V-O) > 2 Å).[52] Therefore the connectivity of vanadium (V) polyhedra (octahedral, square pyramids, trigonal bipyramids or tetrahedra) by sharing corners or edges leads to the building-up of layered structures.[52] The anisotropic arrangement of the vanadium centres in the structure of vanadium (V) oxides with short V-V distances in one or two directions and longer V-V distances in the third distance impacts directly the growth process of the nanocrystals, as a result of the correspondence of the crystalline structure and the morphology of crystallite. As an example for $V_2O_5.nH_2O$ gels, the growth of ribbonlike particles along the *b* axis is related to the crystalline structure of these gels which consist of V_2O_5 nanosheets.[28] The VO_6 octahedra share edges to from double chains along the *b* axis that arrange in parallel and side by side via interchain V-O bonds (by sharing corners of octahedra). In this connectivity motif, intrachain V-O bonding is more extensive than interchain one.[28] Similarly, for numerous V_2O_5 nanowire, nanorods or nanobelts reported, the growth of nanocrystals occurs along the [010] direction.[11,17,42,53] It is also worth noticing that for a large number of $M_2V_6O_{16}$ nanobelts, the anisotropic crystal growth occurs along the [010] direction.[19,46,48,51]

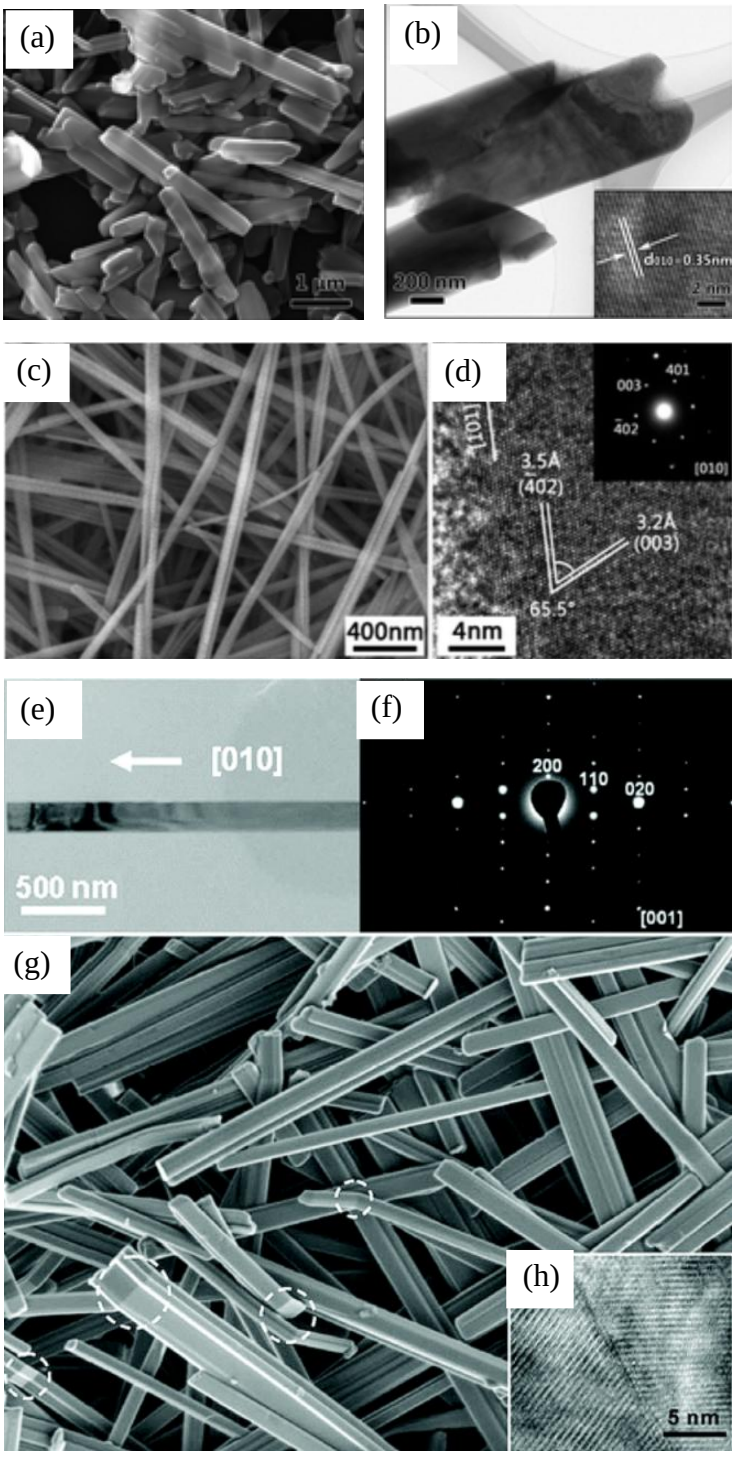

Fig. 7 Vanadium (V) oxides nanostructures. (a) SEM and (b) TEM images of β-$Li_XV_2O_5$ nanorods. The inset in (b) is the HRTEM image of β-$Li_XV_2O_5$ nanorods;[17] (c) SEM and (d) HRTEM and selected area electron diffraction (SAED) pattern of $Ag_{0.33}V_2O_5$ nanowires;[15] (e) TEM image and, (f) the corresponding SAED pattern of a $NH_4V_3O_8$ nanobelt, (g) SEM image of bent or twinned $NH_4V_3O_8$ nanobelts, which are marked by circle, (h) the representative HRTEM image of the twin boundary present in a nanobelt. For (e)-(h) Reprinted with permission from L. Q. Mai, C. S. Lao, B. Hu, J. Zhou, Y. Y. Qi, W. Chen, E. D. Gu, Z. L. Wang, *J. Phys. Chem. B Lett.*, 2006**, 110**, 18138 Copyright (2006) American Chemical Society.[46]

The structure of $K_2V_6O_{16}.1.5H_2O$ (see Fig. 4(b)) consists of infinite V-O chains along the b axis with short V-V distance of 0.18 nm which means that [010] corresponds to a direction with the highest stacking density.[48] In contrast, the longer average V-V distances along the a and c axes respectively close to 0.30 nm and 1.12 nm indicate that both [100] and [001] directions are characterized by a lower stacking densities and slow growth rates are observed in these directions.[48]

3.2 Controlled growth of vanadium oxide nanocrystals: synthesis and formation mechanism of nanowires, nanorods and nanobelts.

In aqueous solution, one-dimensional nanocrystals of $V_2O_5.nH_2O$, $MV_3O_8.nH_2O$ and $M_xV_6O_{16}.nH_2O$ are generally synthesised in solution by combining the sol-gel process and hydrothermal conditions. Hydrothermal reactions are carried out typically in the temperature range 100-250°C under autogeneous pressure and affords a significant number of advantages for the preparation of materials, due to the dependence of the physico-chemical properties of water with temperature and pressure. By increasing temperature and pressure, the dielectric constant of water and its viscosity decrease while its ionization constant significantly increases.[26] Therefore, under these conditions, the solubilisation and diffusion processes of organic and inorganic species are significantly enhanced, thereby impacting the degree of supersaturation of solutions and thus the nucleation step. While strong electrolytes are completely dissociated in water at room temperature, ion-pairs or complexes of low ionic charge can be formed in hydrothermal conditions.[26] As a consequence, under such nonequilibrium crystallization conditions, redissolution-precipitation processes may occur and the nucleation of metastable kinetic phases rather than the thermodynamic ones may be favoured.[26,54]

In the case of nanocrystals of $V_2O_5.nH_2O$, $MV_3O_8.nH_2O$ and $M_2V_6O_{16}.nH_2O$, the synthesis is generally based on the hydrothermal treatment of an acidic vanadate solution at pH 1-3.[14-19,40-51] This vanadic solution which contains a mixture of $[H_2V_{10}O_{28}]^{4-}$ and $[VO_2]^+$ is similar to the initial solution that polymerizes into $V_2O_5.nH_2O$ gel or $MV_3O_8.nH_2O$ (and $M_2V_6O_{16}.nH_2O$) phases (see vide supra).[29,35] This solution can be prepared by acidification of $NaVO_3$ with a mineral acid (HCl, H_3PO_4,…), dissolution of V_2O_5 in water or reaction of V_2O_5 with H_2O_2. The solution can also be prepared through the oxidation of a V(IV) precursor such as VO_2, $VO(acac)_2$ or $VOSO_4$ in acidic condition.[50,55,56] The pH of this initial vanadate solution and the presence of cations are the crucial parameters that determine the chemical nature of the vanadium oxides. For pH in the range 1-1.5 and without foreign cation, one-dimensional nanocrystals of V_2O_5 are typically obtained while those of $MV_3O_8.nH_2O$ (and $M_2V_6O_{16}.nH_2O$) are generally rather isolated with a slightly more alkaline precursor vanadic solution (pH 2-5) with a significant amount of cations.[14-19,40-51] However, it is noteworthy that under hydrothermal conditions, due to the increase of the ionization constant of water, the acido-basic properties of molecular and ionic species may be modified.

For a few one-dimensional nanocrystals of $V_2O_5.nH_2O$, MV_3O_8 and $M_2V_6O_{16}$, the synthesis is very simple and the reaction medium contains only the vanadate precursor and eventually additional ions (i. e. Na^+, K^+ and Cl^-). A typical synthesis of $K_2V_6O_{16}.1.5\ H_2O$ nanobelts consists to acidify a K_3VO_4 solution with HCl to a solution of pH 3, followed by heating in an autoclave at 200°C for about 24 h.[48] In contrast for other vanadium (V) nanocrystals, the synthesis implies the concomitant presence of complexing molecules (MeOH, EtOH, acetylacetonate, citric acid, oxalic acid, fluorure…) or anions (PO_4^{3-}, HSO_4^-) that may covalently interact with the vanadium centres.[14,18,19,41,43,49,57] These complexation reactions may compete with the polymerization of V(V) and/or may affect the nucleation and growth processes of vanadium (V) nanocrystals in solution. The influence of the ethanol

concentration on the microstructure and composition of vanadium oxide nanocrystals obtained hydrothermally was evidenced: for low ethanol concentrations, $H_xV_2O_5.nH_2O$ nanorods were obtained while for larger ethanol concentrations, nanorods or nanosheets of mixed valence vanadium oxides (i. e. $V_3O_7.H_2O$) or VO_2 were isolated.[43] One has to bear in mind that organic additives such as alcohol may also act as reductant of V^{5+} and the presence of V^{4+} in the reaction medium may also affect the nucleation and growth rates of nanocrystals. Actually, it has been reported that V^{4+} serve presumably as catalytic centres for the polymerization of $V_2O_5.nH_2O$ gels.[58]

The nucleation and growth process of oxide crystallites is generally explained by the classical Ostwald Ripening (OR) mechanism which involves the growth of larger particles at the expense of smaller ones.[59,60] It is known that the size and morphology of particles depend on the relative growth of the different crystal facets which is directly linked to their surface energy. The nature of the crystal surface that dominates at the end of the growth process depends on the relative rates of growth of the different crystal facets.[60] The more slowly growing facets are present at the end of the growth process while the faster growing facets are eliminated due to their high surface energy. It is quite known that the growth of primary particles may be strongly influenced by the surrounding medium (acidity, ligands, solvent…) since the different crystal facets may present different surface chemistry and charge (different surface oxygen groups) and thus different surface energy.[26]The complexation or adsorption of one of these facets by molecular or ionic species may enhance their stability and drive the growth process of the nanocrystals. For a few vanadium (V) oxide nanostructures, the time-dependent morphology of the nanocrystals was investigated by TEM along the hydrothermal process. For very long V_2O_5 nanobelts, the careful observation of high-resolution TEM pictures suggest that the nanostructures do not really grow from the OR model, but by aggregation of the primary nanofibers (see Fig. 8).[12] According to the TEM images of small

nanobelts obtained at the early growth stage (Fig. 8), it is possible that the microstructure of some nanobelts result from the crystallite fusion of small nanofibres along the longitudinal direction (see Fig. 8).[12] In some TEM pictures, a stacking of a few nanobelts suggest laterally Oriented Attachment (OA) growth mechanism whose driving force is the reduction of the surface energy.[12] However, the clear determination of the nucleation mechanism would require additional experiments and it is noteworthy that other nucleation mechanisms such as the self-epitaxial nucleation-mediated assembly reported for the formation of biomaterials such as hydroxyapatite[61] may explain the growth of V_2O_5 nanobelts.

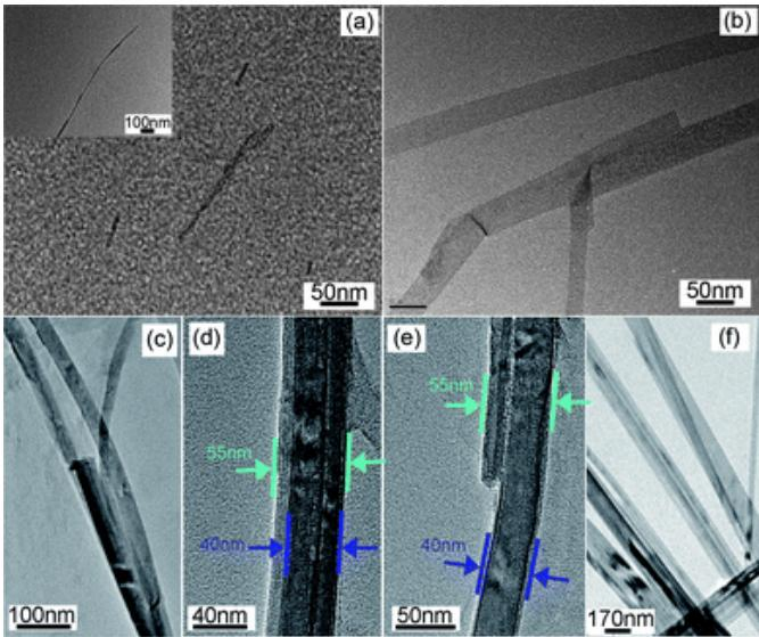

Fig. 8 TEM images of V_2O_5 nanostructures at different growth stages. (a) The as prepared fresh inorganic V_2O_5 sol. The inset shows a single V_2O_5 fiber aged for half a year. (b) TEM image of belt-like structure after hydrothermal treatment of the fresh sol at 220 °C for 1 h. (c), (d) and (e) different parts of an individual V_2O_5 nanobelt after hydrothermal treatment for 2 h. (f) TEM image of V_2O_5 nanobelt after hydrothermal treatment for 6 days.[12]

A similar OA mechanism was also reported for the growth of ultrathin single-crystalline $V_2O_5.0.76$ H_2O nanosheets whose growth results from the lateral aggregation of monocrystalline nanodiscs followed by an epitaxial recrystallization.[62] Initially reported by Penn and Banfield[63] in order to explain the crystallization of one-dimensional single crystalline nanomaterials, this mechanism is based on oriented aggregation and epitaxial

assembly. First, primary nanocrystals interact and form loosely bound aggregates composed of randomly oriented nanocrystals. These aggregates can rearrange and some irreversible attachments between these nanocrystals along some preferential crystallographic orientations lead to nanocrystals such as wires, rods and branched secondary crystals.[59,60] After this OA process, the original microstructural properties of the primary nanocrystals is preserved as well as the interfacial defects. While the driving force of the OA has not been clearly identified, the decrease of the overall surface energy is a possible explanation by eliminating some facets with high surface energy. It is also noteworthy that the presence of capping ligands may also facilitate this OA process.[59,60]

3.3 Spontaneous polarization-induced self-coiling process of nanobelts into nanorings.

Magnetic semiconductor nanoring structures have recently attracted a strong interest due to their combination of semi-conducting and ferromagnetic properties. They present a well-defined and reproducible magnetic state which is suitable for the building-up of spintronic devices. The polycrystalline nanorings, resulting from the assembly of different nanoparticles can be considered as multiple-domain structures. In contrast, the single-crystalline nanorings which result from the self-coiling of nanobelts correspond usually to single-domain structures and are more interesting than their polycrystalline analogs due to the possibility of controlling the spin of electrons by manipulating the flux current.[50,51] The understanding of the growth process of single-crystalline nanorings would offer new opportunities to design single-crystalline magnetic semiconductor nanorings.

For a few vanadium oxide nanobelts such as $(NH_4)_{0.5}V_2O_5$, $Na_2V_6O_{16}.3H_2O$, $Ag_{1.2}V_3O_8$,[14,49,50,51] their hydrothermal synthesis leads also to a significant amount of nanorings. This mixture nanobelts/nanorings is obtained in the same experimental conditions than pure nanobelts and synthesized through the hydrothermal treatment of an acidic vanadate

solution. In some cases, complexing ligands (H_3PO_4, acethylacetonate, citric acid…) are also present in the reaction medium. While the nanobelt morphology prevails generally in the samples, a significant amount of nanorings with a perfect circular shape and a diameter between 1 and 7 μm are also present,[14,49-51] together with more complex loop-like ring structures (i. e. $Na_2V_6O_{16}.3H_2O$, $Ag_{1.2}V_3O_8$)[50,51] or even triangles ($(NH_4)_{0.5}V_2O_5$).[14] (Fig. 9) For $Ag_{1.2}V_3O_8$ and $Na_2V_6O_{16}.3H_2O$, two kinds of loops with hollow cavities are evidenced on the TEM pictures: microtube-like loop with a uniform diameter along the whole tube (left top of Fig. 9(b)) and nanoloop with a varied diameter along the tube (left bottom of Fig. 9(b)). A possible mechanism for the formation of vanadium (V) oxides nanorings is based on the spontaneous self-coiling of polar nanobelts which requires long-range electrostatic interactions for the circular folding of the nanobelts and then short-range chemical bonds among loops to form the single-crystalline rings.[50,51] According to the HRTEM images, $Na_2V_6O_{16}.3H_2O$ nanobelts grow along the [010] direction and exhibit the surface face (100) and side face (001).[51] According to the atomic models based on the crystalline structure of

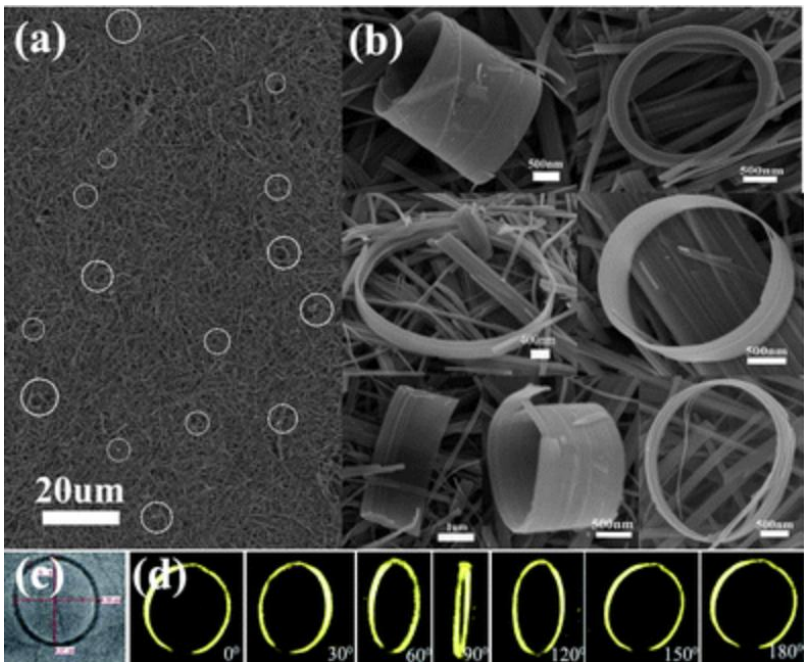

Fig. 9 (a) Low- and (b) high-magnification FESEM images of the as-prepared $Na_2V_6O_{16}·3H_2O$ nanobelts and nanorings. (c) Two dimensional and (d) three dimensional imaging of a nanoring recorded by X-ray nanotomography.[51]

$Na_2V_6O_{16}.3H_2O$, both (100) an (001) are polar surfaces. The ±(100) plane is terminated either by $[V_3O_8]^-$ or Na^+ surfaces while the ±(001) plane either by $[Na_2V_2O_5]^{2+}$ or $[V_4O_{11}]^{2-}$ as shown in Fig 10.[51] Therefore, the $Na_2V_6O_{16}.3H_2O$ nanobelts bear a pair of positively and negatively charged polar surfaces giving rise to two self-coiling configurations. In one possible configuration, the coiling of nanobelt occurs side-by-side by stacking (001) plane (Fig. 10(d)). This mechanism may explain the perfect nanoring structure as shown in the upper-left of Fig. 9(b).[51] In another configuration, the stacking of (100) planes (Fig. 10(e)) leads to tape-like nanoring structure (see upper-right of Fig.9(b)). Furthermore, more complex loop-like morphologies are formed and may be explained by the synergetic effects of stacking both (100) and (001) planes.[51] It is noteworthy that the driving force of the self-coiling is the predominance of the electrostatic energy over the elastic energy. As a consequence, only the polar surfaces with a sufficient density of positive and negative charge pairs will be involved in self-coiling mechanism since the corresponding electrostatic energy induced by the charge polarization has to be larger than the elastic energy for the roll-up process to proceed. This is the reason why (010) polar surfaces of $Na_2V_6O_{16}.3H_2O$ are not involved in the self-coiling process.[51]

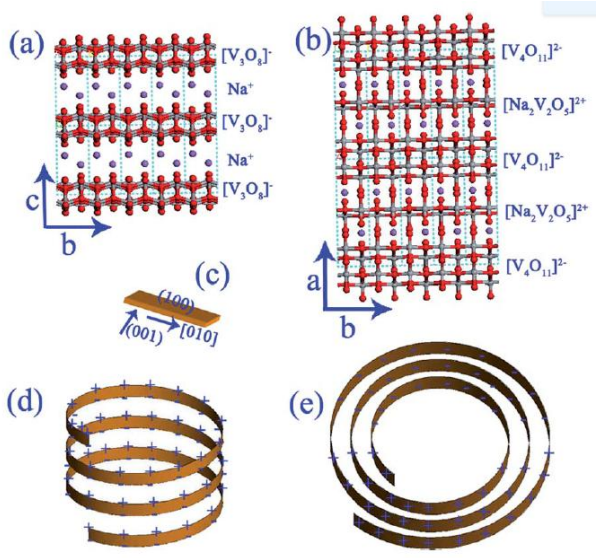

Fig. 10 The intrinsic polarity of the crystal along the c-axis (a) and the a-axis (b). (c) The schematic image of a $Na_2V_6O_{16}\cdot 3H_2O$ nanobelt. (d, e) The schematic mechanism of self-coiling polar nanobelts stacking in both ±(001) (d) and ±(100) (e) planes.[51]

This hypothesis explains also the low amount or absence of nanorings structures among the samples of nanobelts (i. e. $(NH_4)_2V_6O_{16}.3H_2O$ or $K_2V_6O_{16}.5H_2O$ with a direction of growth along [100]) for which the electrostatic interactions between polar surfaces is not sufficient to induce an electrostatic energy able to compensate the elastic energy.[51]

4. Hydrothermal synthesis of VO_x nanotubes

Among nanostructured vanadium oxides, Nesper and co-workers first reported vanadium oxide nanotubes (VO_x-NT) which correspond to vanadium oxide-amine composites with a nanoscale scroll-like structure.[1b,20,64] These tubular materials were synthesized by combining sol-gel polymerization reactions of vanadium precursor and ligand-assisted templating methods.[20,65,66,67] The tube walls consist of crystalline vanadium oxide layers with amine templates intercalated in between (see Fig. 11).[68] The nanotube morphology is either constructed in closed concentric cylinders or formed by scrolling one or more layers. The number of layers depends on the chemical nature of the template: monoamines lead to thin walls (2-10 layers) while diamines yield predominantly thick walls consisting of more than 10 layers.[20,65] Petkov *et al* proposed a model of the VO_x-NT structure according to the PDF technique, suggesting that the layered structure of VO_x-NT is apparently close to that of BaV_7O_{16}.[69] This structure consists of an assembly of double layers of VO_5 square pyramid units connected by VO_4 tetrahedra.

In comparison with other tubular systems, VO_x-NT exhibit interesting interfacial properties as a consequence of four different contact regions i.e. tubes opening, outer and inner surfaces, interstitial region. Therefore, the building-up of nanodevices based on VO_x-NT for energy storage/release applications has stimulated intense research. More specifically, VO_x-NT have been extensively studied as positive electrodes for Li-batteries and discharge capacities as high as 200 mAh/g have been measured.[70] However, their large degree of disorder hampers

their mechanical and electrical behavior. The magnetic, optical and dielectric properties of VO_x-NT were also deeply investigated.[71,72,73] Furthermore, copper nanoparticles embedded in VO_x-NT were studied for potential applications in catalysis.[74] VO_x-NT were also used as precursors for the design of vanadium sulfide nanotubes.[75] The nucleation and growth of hollow centered microspheres composed of radially oriented VO_x-NT (nano-urchin structures) was also reported.[76]

The synthesis, characterization, electrochemical properties of VO_x-NT were recently reviewed by Mc Nulty *et al*.[6] The present part of this paper will be more specifically focused on the growth mechanism of these nanomaterials. Since the discovery of these VO_x-NT in 1998, a tremendous interest has been devoted to the determination of the chemical and physical parameters (molar ratio, duration of the hydrothermal process, ageing time…) influencing their formation since this knowledge would offer new opportunities to design nanomaterials with anisotropic morphology. Numerous synthesis protocols of VO_x-NT have been reported to date and have in common to be based on the intercalation of long-alkyl chain amines into a V_2O_5 phase followed by an hydrothermal treatment at 180°C for about 7 days. These procedures are distinguished by the nature of the V_2O_5 phase that can be either the crystalline V_2O_5 powder or a V_2O_5 gel.[20,65,66,67] Aqueous V_2O_5 gels could be prepared by the classical sol-gel methods including the reaction of H_2O_2 with V_2O_5,[67] the acidification of $NaVO_3$,[66] the hydrolysis of $VOCl_3$[20b] or melting-quenching of V_2O_5.[77] Organic V_2O_5 gels were also prepared through the hydrolysis of vanadium alkoxides ($VO(OPr^i)_3$).[20a,65a,65b] More recently, a molecular vanadium (IV) precursor (i. e. $VO(acetate)_2$) was also used and its partial oxidation with oxygen under hydrothermal conditions in a solution of dodecylamine, ethanol and water could also lead to VO_x-NT.[78] The VO_x-NT produced by these different strategies present similar crystalline structure and microstructure. However, a comparison of the characterization of VO_x-NT synthesized from the mixture of H_2O_2 with V_2O_5 with those

prepared from powder V_2O_5 has shown that the former present certainly a larger water rate and V^{4+}/V^{5+} ratio.[79] The remarkable feature of the VO_x-NT synthesis is related to the possibility of using a large number of vanadium precursors and this result suggests that a similar growth mechanism of VO_x-NT occurs certainly during all these synthetic procedures.

(A)

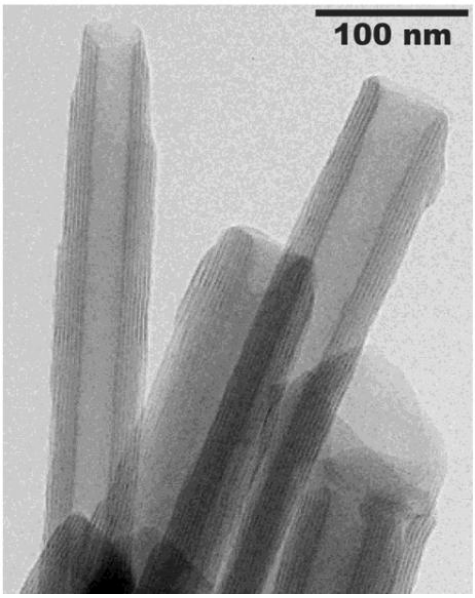

(B)

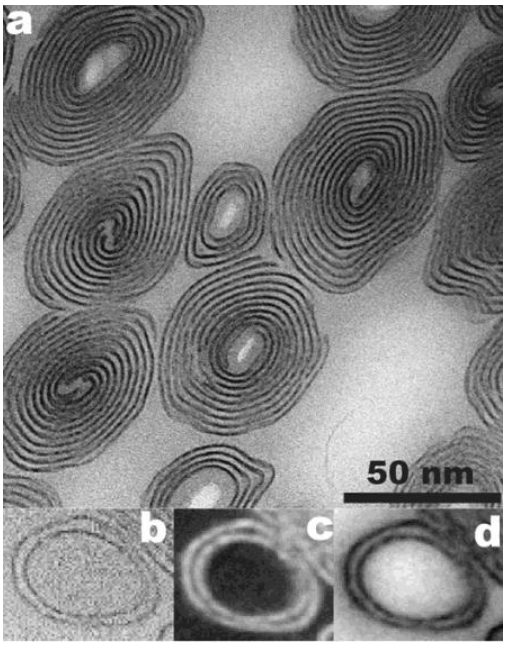

Fig. 11 (A) Typical TEM image of VO_x-NTs (template: docosylamine); (B) Cross-sections of VO_x-NTs (template: hexylamine). a,b) TEM images, b-d) Tube consisting of two concentric cylinders of VO_x layers.

c) Vanadium map, V-containing sites appear bright. d) Carbon map, C-containing sites appear bright. Vanadium and carbon distributions occur in distinctly alternating regions in the wall regimes. (Reproduced from [64] with permission from John Wiley & Sons.)

It has been clearly shown by powder X-ray diffraction that the first step of the VO_x-NT formation implies the intercalation of amines into the interlamellar space of crystalline or amorphous V_2O_5.[20,67] One of the first mechanism regarding the rolling process of VO_x-NT was proposed by Chen *et al*.[66] It was proposed that if, during the hydrothermal treatment the lamellar sheets became loose at the edges and the corresponding interlayer interactions decrease from the edges then the rolling process could take place.[66] The lower the surfactant content, the weaker the interactions between surfactant and vanadium oxide layers as well as the weaker the Van der Waals interactions between the surfactant tails should be. Therefore, the rolling of vanadium oxide sheets should take place as a result of an insufficient amount of surfactant electrostatically combined with the layers.

This hypothesis was supported by recording TEM images on reactional intermediates isolated at different duration of the hydrothermal process.[66] According to the change of colour from the V_2O_5 precursor to VO_x-NT, a partial reduction of V^{5+} to V^{4+} during the hydrothermal process was hypothesized and confirmed by recording a XPS spectrum of VO_x-NT.[77] Sun *et al* suggested that this V^{4+}/V^{5+} ratio plays a significant role in the microstructure of VO_x-NT as well as their growth process.[80] First, reducing conditions have an impact on the presence of structural defects (i. e. cracks in the walls) in VO_x-NT. Nearly perfects scrolls are isolated under highly reducing conditions while nanorolls with many cracks in the oxide walls are obtained under moderate reducing conditions.[80] Furthermore, it is noteworthy that the anionic charge density on the vanadium oxide wall is a direct function of the V^{4+} content: the higher the anionic charge on the wall is, the larger amount of cationic surfactant that can be associated with the composite.[80] As previously reported for surfactant template syntheses of metal oxides,[81] the formation of VO_x-NT proceeds certainly through a cooperative mechanism

combining the self-assembly of amines and the polymerization of vanadium centres, meaning that the final nanostructure is driven by the interplay between surfactant packing and charge density matching between the amines and the vanadium oxide sheets. As reported for silica, a high density of surfactant in interaction with a high negatively charged silica, is most effectively observed for a low (negative) curvature structure at the silica/surfactant interface.[81,82] Thus, surfactant headgroup density contributes to drive the overall composite structure.

A mechanism of the rolling process was also proposed by Vera-Robles *et al* for VO_x-NT synthesized from the $V^{IV}O(acetate)_2$.[78] According to XRD, these nanotubes are structurally identical to those obtained by other chemical routes despite of the fact that their formation implies an oxidation of V^{4+} instead of a reduction of V^{5+}. Therefore, the partial reduction of V^{5+} to V^{4+} is not the crucial step to induce the formation of VO_x-NT but the key step is to achieve an appropriate V^{4+}/V^{5+} ratio presumably close to 1 that may trigger the scrolling process of vanadium oxide sheets.[78] Since the chemical parameters such as pH, temperature and duration of the hydrothermal process as well as the vanadium/amine ratio may influence the V^{4+}/V^{5+} ratio, these parameters have to be precisely controlled during the synthesis. Actually, it has been clearly shown that VO_x-NT are strictly obtained in some peculiar physico-chemical conditions.[20,64-67,83] For an hydrothermal treatment with a temperature lower than 180°C or a duration lower than 7 days, no VO_x-NT are formed. Moreover, the V/amine molar ratio has to be fixed to 2 for the preparation of VO_x-NT.[20,67] Finally, Vera-Robles *et al* has proposed a mechanism in three steps: i) the formation of a vanadium oxide-dodecylamine composite, ii) the partial oxidation of V^{4+} to V^{5+} during the hydrothermal process, iii) for a V^{4+}/V^{5+} ratio close to 1, the scrolling process is triggered and VO_x-NT are formed.[78]

In order to better understand the crystallization and growth mechanism of VO_x-NT, we have followed the formation of vanadium oxide nanotubes along the hydrothermal treatment

by several ex-situ techniques.[83] Time-resolved in-situ techniques could not be used because of the complexity and gradual changes of the reaction medium (different molecular species and solid phases) along the hydrothermal synthesis of VO_x-NT. Nevertheless, the nature of the various intermediate phases, at different reaction times, could be monitored by ex-situ characterization, in relation with the solution speciation.[83] For that purpose, small aliquots of the reaction medium were sampling at different reaction times, followed by reaction quenching and characterization. Therefore, a series of fourteen samples from the initial V_2O_5-hexadecylamine (HDA) composite to the final VO_x-NT were extracted at different stages of the hydrothermal process and characterized by powder X-ray diffraction, X-ray absorption near-edge structure (XANES) at the V K-edge, electron spin resonance (ESR) and electron microscopy (SEM and TEM).[83] The starting $V_2O_5.nH_2O$ gel was prepared by dissolution of the V_2O_5 powder with H_2O_2.[67] The first step implies the intercalation of amines into the interlamellar space of $V_2O_5.nH_2O$ gels. This intercalation step which proceeds through proton-exchange reactions is much easier than in crystalline V_2O_5. Therefore this step is notably shorter (16 h) than in other chemical syntheses for VO_x-NT. The characterization of the different samples along the hydrothermal process has clearly shown the presence of two vanadium oxide phases.[83] For a hydrothermal treatment less than 24 h, a lamellar and hydrated V_2O_5-HDA intercalate with a poor crystallinity is first formed. After a hydrothermal process of 24 h, this lamellar phase is progressively converted into vanadium oxide nanotubes whose crystallinity and amount increase by heating further from 1 to 7 days. According to XRD, a significant dehydration of the vanadium oxides occurs during this transformation and should be inherent to the presence of long alkyl chain amines that are rather prone to solubilize hydrophobic compounds. By flame spectroscopy titration, an increase of the vanadium and amine concentrations in the supernatant solutions is clearly observed beyond 100 hours of hydrothermal treatment.[83] The release of amines in solution out of the vanadium

oxide layers is consistent with an increase of the V/N ratio (determined by chemical analyses) of solids along the hydrothermal process.[83] Moreover, by recording ^{51}V NMR spectra at 100°C on supernatant solutions obtained after heating V_2O_5-HDA intercalate at 180°C for different durations (from 2 h to 7 d), metavanadates $[H_nVO_4]^{(-3+n)}$ and cyclic metavanadates $[V_4O_{12}]^{4-}$/$[V_5O_{15}]^{5-}$ could be evidenced in solution.[83] These results are consistent with a redissolution-precipitation mechanism which would imply a progressive dissociation of the vanadium-oxide intercalates and the crystallization of VO_x-NT. The diffusion of amines out of the interlayer region is certainly favored by an increase of their solubilization under hydrothermal conditions due to the decrease of the dielectric constant of water and the increase of its ionization constant. Such a redissolution-precipitation process may explain why VO_x-NT can be formed from a wide range of molecular or solid vanadium precursors of different chemical structure and reactivity, including vanadium oxide foams.[83,84] These results show that the initial vanadium precursor is not expected to influence strongly the formation of VO_x-NT as soon as it can be converted to a molecular polyoxovanadate species that can condense into VO_x-NT. Controlling synthesis parameters such as temperature, pH, duration of the hydrothermal process, vanadium/amine ratio is crucial since these parameters are directly involved in chemical equilibria between polyoxovanadate species and linked to the speciation of V^{5+} (and V^{4+}) species in aqueous solution.

A strong reduction of V^{5+} during the first 24 h of the hydrothermal process was clearly shown by ESR and XAS experiments and a correlation between gel dehydration and vanadium reduction is currently observed during the formation of VO_x-NT, showing the complex role of water in the vanadium oxide formation.[83] Apparently, amines have a much more complex role than structure directing agents. As Brönsted bases and hydrophobic molecules, they certainly favor both dehydration of vanadium pentoxide gels and reduction of V^{5+}.[78,83] Finally, it was proposed that VO_x-NT result from the ring-polymerization (ROP) of

cyclic metavanadates $[V_4O_{12}]^{4-}$. This hypothesis was supported by the previously reported synthesis of the mixed-valence TMA$[V_4O_{10}]$ from TMAOH and V_2O_5 precursors.[85] ^{51}V NMR spectra were recorded on supernatant solutions from which crystals of TMA$[V_4O_{10}]$ were grown. These solutions contain some decavanadates $[H_nV_{10}O_{28}]^{(6-n)-}$ (δ = -427, -502 and -518 ppm) and cyclic metavanadates (*i.e.* $[V_4O_{12}]^{4-}$ at δ = -582 ppm and $[V_5O_{15}]^{5-}$ at δ = -591 ppm). By increasing temperature, the molecular ratio [decavanadate]/[metavanadate] decreases progressively from 91/9 at RT to 76/24 at 100°C.[85] At a given temperature, it also decreases as a function of the heating time. According to in-situ ^{51}V NMR experiments the equilibrium (eq.1) between decavanadate and metavanadate species is thus progressively displaced toward the formation of $[V_4O_{12}]^{4-}$.[85]

$$2[H_2V_{10}O_{28}]^{4-} + 4H_2O \leftrightarrow 5[V_4O_{12}]^{4-} + 12H^+ \qquad (1)$$

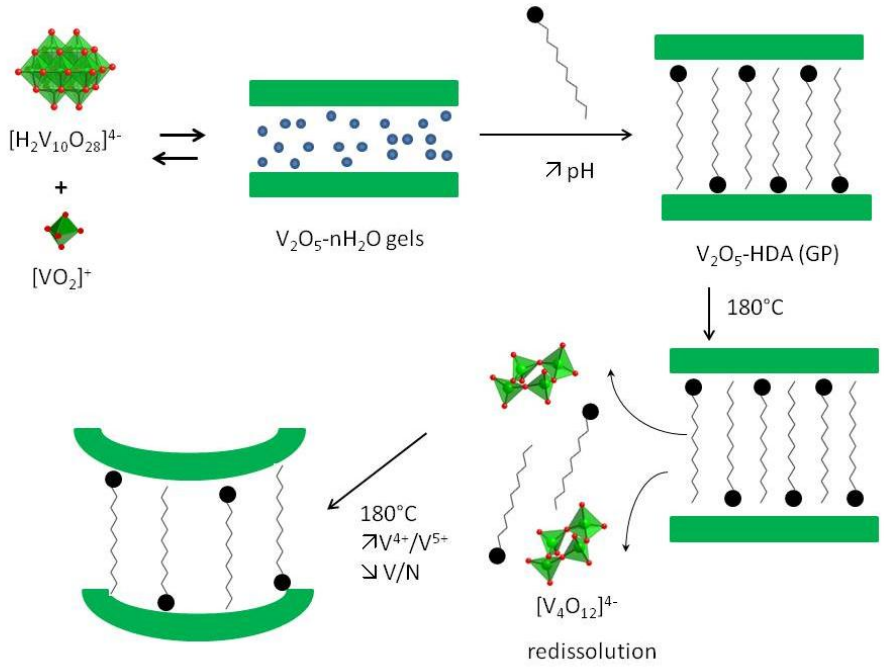

Fig. 12. Mechanistic scheme representing the main steps of the VO_X-NT formation. Reprinted with permission from M. Jaber, F. Ribot, L. Binet, V. Briois, S. Cassaignon, K. J. Rao, J. Livage, N. Steunou, *J. Phys. Chem. C*, 2012, **116**, 25126. Copyright (2012) American Chemical Society.[83]

In the case of VO_x-NT formation, since cyclic metavanadates $[V_4O_{12}]^{4-}$ have been detected by ^{51}V NMR, a transformation of decavanadates into metavanadates may take place during the hydrothermal process. Actually, $V_2O_5.nH_2O$ gels are in equilibrium with $[H_2V_{10}O_{28}]^{4-}$ and $[VO_2]^+$ polyoxovanadates and the alcalinization of the reaction medium through the addition of amines may favor the conversion of decavanadates into metavanadates. It may then be assumed that these metavanadates behave as molecular precursors for the layered structure of VO_x-NT.[83] Since protons are formed when decavanadates are converted into metavanadates (eq.1), protonation of vanadate precursors may be followed by the vanadium condensation and coordination expansion. A possible mechanistic scheme was provided (see Fig. 12).[83]

5. Summary and outlook

Vanadium pentoxide (V_2O_5) has been in the forefront of applied research due to its fascinating physical properties such as electronic, optical, electrochromic, photochromic and photocatalytic. For the building-up of novel nanodevices, the nanostructures of V_2O_5 have attracted a tremendous interest in different fields of application including Li-ion batteries,[6,7,86] field effect transistors,[87] chemical and biosensors,[35,88] supercapacitors,[89] waveguides,[90] actuators.[91] The electrochemical properties of V_2O_5 are certainly the most significant ones from a practical point of view. Numerous low-dimensional V_2O_5 (or MV_3O_8 and $M_2V_6O_{16}$) nanostructures including nanorods, nanowires, nanobelts, nanotubes, nanorings and nanosheets have been synthesized by different approaches. In the present article, we have outlined the different chemical routes in solution that combine hydrothermal processes and sol-gel synthesis in order to distinguish the chemical and physical parameters driving the crystallization of these nanostructures. The examples covered within this review tend to emphasize how the control of the composition of the reaction medium (nature of precursors, presence of complexing ligands, molar ratio…) as well as the synthesis parameters (pH,

temperature, duration, ageing..) is important to tune the nature of the vanadium oxide, its crystallinity and morphology (size, shape, aspect ratio). In reason of their ionic character, the 2D layered structure of metal oxides is usually very stiff and therefore its folding into nanotubes is quite demanding in terms of the elastic energy compared to the quite flexible MoS_2 structure.[92] This is the reason why the nanoscroll morphology of VO_x-NT is particularly fascinating and the flexibility of this composite arises certainly from the presence of amines. Numerous low-dimensional V_2O_5 (or MV_3O_8 and $M_2V_6O_{16}$) nanocrystals present significant advantages in terms of electrochemical kinetics, ionic and electronic conductivity. However for a few nanostructures, there are several limitations and shortcomings that result from the high surface energy of nanoparticles. One critical issue is the low volumetric energy density due to the low packing density of the active material in the electrode.[93,94] Moreover, the thermodynamic instability and potential nano-toxicity of nanoparticles associated to the possible high cost of their processing makes the design of microstructurally composed nanoparticle assemblies potentially interesting. Two-dimensional or three-dimensional hierarchical assemblies of V_2O_5 nanoparticles including hollow or porous V_2O_5 microspheres,[95] V_2O_5 nanoflowers,[96] V_2O_5 nanostars[93,94,97], and hollow V_2O_5 nanoparticles[98] have been recently synthesized by several methods including sol-gel and solvothermal synthesis, template synthesis followed by thermal treatment or seeded growth strategy. Recently reported in the literature, crystallographically oriented nanoparticle superstructures or mesocrystals are crystalline solids with crystal facets ranging from a few hundreds nanometres to the micrometre size regime.[60] Their smallest building units correspond to nanocrystals that are arranged along a shared crystallographic register and the inner crystalline structure of mesocrystals is analogous to that of single crystals.[60,94] Since mesocrystals present both nanoparticle characteristics together with those arising from the collective interactions of nanoparticles, a synergism of properties may be expected and is of

great interest for many applications, amongst which are Li-ion batteries especially for vanadium oxide based cathodes.[93,94] Micron-sized mesocrystals of VO_2(B) with an ellipsoidal star topology have been recently reported: their microstructure consists of six arms that are self-assembled from stacked nanosheets 20-60 nm thick and radially aligned with respect to the centre of the architecture.[93,94] The VO_2(B) present a high electrochemical performance in terms of Li-ion capacity which was mainly imparted to the mesocrystalline microstructure. These last examples of hierarchical nanocrystals superstructures open a wide range of perspectives for the building-up of novel nanodevices.

References

[1] (a) J. H. Park, S. Kim, A. J. Bard, *Nano Lett.*, 2006, **6**, 24 ; (b) J. Perez-Carvajal, P. Aranda, A. Berenguer-Murcia, D. Cazorla-Amoros, J. Coronas, E. Ruiz-Hitzky, *Langmuir*, 2013, **29**, 7449 (c) G. R. Patzke, F. Krumeich, R. Nesper, *Angew. Chem. Int. Ed.*, 2002, **41**, 2446

[2] (a) Themed issue: Progress in bionanocomposites: from green plastics to biomedical applications, *Progress in Polym. Sci.*, 2013, **38**, 1389-1772; (b) L. Johnson, W. Thielemans, D. A. Walsh, *Green Chem.*, 2011, **13**, 1686.

[3] S. M. Whittingham, *Chem. Rev.*, 2014, **114**, 11414.

[4] Y. Liu, D. Liu, Q. Zhang, G. Cao, *J. Mater. Chem.*, 2011, **21**, 9969.

[5] F. Cheng, J. Chen, *J. Mater. Chem.*, 2011, **21**, 9841.

[6] D. Mc Nulty, D. N. Buckley, C. O'Dwyer, *J. Power Sources*, 2014, **267**, 831.

[7] Y. Wang, G. Cao, *Chem. Mater.*, 2006, **18**, 2787.

[8] M. S. Whittingham, *J. Electrochem. Soc.*, 1976, **123**, 315.

[9] M. S. Whittingham, *Chem. Rev.*, 2004, **104**, 4271.

[10] R. S. Devan, R. A. Patil, J-H Lin, Y-R. Ma, *Adv. Funct. Mater.*, 2012, **22**, 3326.

[11] (a) N. Pinna, U. Wild, J. Urban, R. Schlögl, *Adv. Mater.*, 2003, **15**, 329 ; (b) N. Pinna, M. Willinger, K. Weiss, J. Urban, R. Schlögl, *Nano Lett.*, 2003, **3**, 1131.

[12] M. Li, F. Kong, H. Wang, G. Li, *CrystEngComm.*, 2011, **13**, 5317

[13] T. Zhai, H. Liu, H. Li, X. Fang, M. Liao, L. Li, H. Zhou, Y. Koide, Y. Bando, D. Golberg, *Adv. Mater.*, 2010, **22**, 2547.

[14] G. T. Chandrappa, P. Chithaiah, S. Ashoka, J. Livage, *Inorg. Chem.*, 2011, **50**, 7421.

[15] Y. Xu, X. Han, L. Zheng, W. Yan, Y. Xie, *J. Mater. Chem.*, 2011, **21**, 14466.

[16] E. Khoo, J. M. Wang, J. Ma, P. S. Lee, *J. Mater. Chem.*, 2010, **20**, 8368.

[17] W.-D. Li, C. -Y. Xu, X. -L. Pan, Y. -D. Huang, L. Zhen, *J. Mater. Chem. A*, 2013, **1**, 5361.

[18] G. -T. Zhou, X. Wang, J. C. Yu, *Cryst Growth Design*, 2005, **5**, 969

[19] J. Yu, J. C. Yu, W. Ho, L. Wu, X. Wang, *J. Am. Chem. Soc*., 2004, **126**, 3422.

[20] (a) F. Krumeich, H. -J.Muhr, M. Niederberger, F. Bieri, B. Schnyder, R. Nesper, *J. Am. Chem. Soc.*,1999, **121**, 8324. (b) M. Niederberger, H. -J. Muhr, F. Krumeich, F. Bieri, D. Günther, R. Nesper, *Chem. Mater.* 2000, **12**, 1995.

[21] (a) H. Shi, Z. Li, J. Kou, J. Ye, Z. Zou, *J. Phys. Chem. C.*, 2011, **115**, 145; (b) F. Sauvage, V. Bodenez, J. -M. Tarascon, K. R. Poeppelmeier, *J. Am. Chem. Soc.*, 2010, **132**, 6778.

[22] K. Takahashi, S. J. Limmer, Y. Wang, G. Cao, *Jpn. J. Appl. Phys.*, 2005, **44**, 662.

[23] D. Yu, C. Chen, S. Xie, Y. Liu, K. Park, X. Zhou, Q. Zhang, J. Li and G. Cao, *Energy Environ. Sci.*, 2011, **4**, 858.

[24] (a) C. K. Chan, H. Peng, R. D. Twesten, K. Jarausch, X. F. Zhang, Y. Cui, *Nano Lett.*, 2007, **7**, 490; (b) J. M. Velazquez, S. Banerjee, *Small*, 2009, **5**, 1025.

[25] J. Prado-Gonjal, B. Molero-Sanchez, D. Avila-Brande, E. Moran, J. C. Perez-Flores, A. Kuhn, F. Garcia-Alvarado, *J. Power Sources*, 2013, **232**, 173.

[26] J. P. Jolivet *De la solution à l'oxyde*, Intereditions, Paris, 1994.

[27] J. Livage, *Chem. Mater.*, 1991, **3**, 578.

[28] V. Petkov, P. N. Trikalitis, E. S. Bozin, S. J. L. Billinge, T. Vogt, M. G. Kanatzidis, *J. Am. Chem. Soc.*, 2002, **124**, 10157

[29] O. Durupthy, N. Steunou, T. Coradin, J. Maquet, C. Bonhomme, J. Livage, *J. Mater. Chem.*, 2005, **15**, 1090.

[30] B. Alonso, J. Livage, *J. Solid State Chem.*, 1999, **148**, 16.

[31] L. Znaidi, N. Baffier and D. Lemordant, *Solid State Ionics*, 1988, **28-30**, 1750.

[32] (a) A. Bouhaouss and P. Aldebert, *Mat. Res. Bull.*, 1983, **18**, 1247; (b) N. Soga and M. Senna, *Solid State Ionics*, 1993, **63-65**, 471; (c) Y. J. Liu, J. L. Schindler, D. C. DeGroot, C. R. Kannewurf, W. Hirpo and M. G. Kanatzidis, *Chem. Mater.*, 1996, **8**, 525; (d) E. Ruiz-Hitzky and B. Casal, *J. Chem Soc., Faraday Trans.*, 1986, **82**, 1597.

[33] (a) H. T. Evans and J. M. Hughes, *Am. Mineral.*, 1990, **75**, 508; (b) A. D. Wadsley, *Acta. Crystallogr.*, 1957, **10**, 261.

[34] O. Durupthy, J. Maquet, C. Bonhomme, T. Coradin, J. Livage, N. Steunou, *J. Mater. Chem.*, 2008, **18**, 3702.

[35] N. Steunou, C. Mousty, O. Durupthy, C. Roux, G. Laurent, C. Simonnet-Jegat, J. Vigneron, A. Etcheberry,C. Bonhomme, J. Livage, T. Coradin, *J. Mater. Chem.*, 2012, **22**, 15291.

[36] Y. Oka, T. Yao, S. Sato, N. Yamamoto, *J. Solid State Chem.*, 1998, **140**, 219.

[37] (a) Y. Oka, T. Yao and N. Yamamoto, *Mater. Res. Bull.*, 1997, **32**, 1201. (b) H. T. Evans and S. Block, *Inorg. Chem.*, 1966, **5**, 1808. (c) A. D. Kelmers, *J. Inorg. Nucl. Chem.*, 1961, **21**, 45. (d) B-Z. Lin, S-X Liu, *Acta Crystallogr., Sect C:Cryst. Struct. Commun.*, 1999, **55**, 1961.

[38] D. Dubarry, J. Gaubicher, D. Guyomard, O. Durupthy, N. Steunou, J. Livage, N. Dupré, C. P. Grey. *Chem. Mater.*, 2005**, 17**, 2276.

[39] M. Henry, J. P. Jolivet and J. Livage, *Struct. Bonding*, 1992, **77**, 153.

[40] X. Wu, Y. Tao, L. Dong, J. Hong, *J. Mater. Chem.*, 2004, **14**, 901.

[41] H. Li, T. Zhai, P. He, Y. Wang, E. Hosono, H. Zhou, *J. Mater. Chem.*, 2011, **21**, 1780.

[42] T. Zhai, H. Liu, H. Li, X. Fang, M. Liao, L. Li, H. Zhou, Y. Koide, Y. Bando, D. Golberg, *Adv. Mater.*, 2010, **22**, 2547.

[43] A. V. Grigorieva, S. M. Badalyan, E. A. Goodilin, M. N. Rumyantseva, A. M. Gaskov, A. Birkner, Y. D. Tretyakov, *Eur. J. Inorg. Chem.*, 2010, 5247.

[44] U. Schlecht, M. Knez, V. Duppel, L. Kienle, M. Burghard, *App. Phys. A*, 2004, **78**, 527.

[45] B. Li, Y. Xu, G. Rong, M. Jing, Y. Xie, *Nanotechnol.*, 2006, **17**, 2560.

[46] L. Q. Mai, C. S. Lao, B. Hu, J. Zhou, Y. Y. Qi, W. Chen, E. D. Gu, Z. L. Wang, *J. Phys. Chem. B Lett.*, 2006, **110**, 18138.

[47] S. Liang, J. Zhou, G. Fang, J. Liu, Y. Tang, X. Li, A. Pan, *ACS Appl. Mater. Interfaces*, 2013, **5**, 8704.

[48] L. Bai, Y. Xue, J. Zhang, B. Pan, C. Wu, *Eur. J. Inorg. Chem.*, 2013, 3497.

[49] P. Chithaiah, G. T. Chandrappa, J. Livage, *Inorg. Chem.*, 2012, **51**, 2241.

[50] C. Wu, H. Zhu, J. Dai, W. Yan, J. Yang, Y. Tian, S. Wei, Y. Xie, *Adv. Funct. Mater.*, 2010, **20**, 3666.

[51] Y. Xue, X. Zhang, J. Zhang, J. Wu, Y. Sun, Y. Tian, Y. Xie, *J. Mater. Chem.*, 2012, **22**, 2560.

[52] P. Y. Zavalij, M. S. Whittingham, *Acta. Crystallogr. Sect B*, 1999, **55**, 627.

[53] D. Su, G. Wang, *ACS Nano*, 2013, **7**, 11218.

[54] P. J. Hagrman, R. C. Finn, J. Zubieta, *Solid State Sci.*, 2001, **3**, 745.

[55] D. M. Minic, V. A. Blagojevic, *CrystEngComm.*, 2013, **15**, 6617.

[56] (a) F. Natalio, R. André, S. A. Pihan, M. Humanes, R. Wever, W. Tremel, *J. Mater. Chem.*, 2011, **21**, 11923; (b) R. André, F. Natalio, M. Humanes, J. Leppin, K. Heize, R. Wever, H.-C. Schröder, W. E. G. Müller, W. Tremel, *Adv. Funct. Mater.*, 2011, **21**, 501.

[57] H. Wang, S. Liu, Y. Ren, W. Wang, A. Tang, *Energy Environ. Sci.*, 2012, **5**, 6173.

[58] C. A. Poznarsky, A.V. McCormick, *Chem. Mater.*,1994, **6,** 380.

[59] X. Xue, R. L. Penn, E. R. Leite, F. Huang, Z. Lin, *CrystEngComm.*, 2014, **16**, 1419.

[60] L. Bahrig, S. G. Hickey, A. Eychmüller, *CrystEngComm.*, 2014, **16**, 9408.

[61] (a) Z. Wang, G. Ma, X. Y. Liu, *J. Phys. Chem. B*, 2009, **113**, 16393 ; (b) X. Y. Liu, S. W. Lim, *J. Am. Chem. Soc.*, 2003, **125**, 888.

[62] X. Rui, Z. Lu, Z. Yin, D. H. Sim, N. Xiao, T. M. Lim, H. H. Hng, H. Zhang, Q. Yan, *Small*, 2013, **9**. 716.

[63] (a) R. L. Penn, J. F. Banfield, *Science*, 1998, **281**, 969; (b) J. F. Banfield, S. A. Welch, H. Zhang, T. T. Ebert, R. L. Penn, *Science*, 2000, **289**, 751.

[64] H.-J. Muhr, F. Krumeich, U. P. Schönholzer, F. Bieri, M. Niederberger, L. J. Gauckler, R. Nesper, *Adv. Mater.*, 2000, **12**, 231.

[65] (a) F. Bieri, F. Krumeich, F. H.-J. Muhr, R. Nesper, *Helv. Chim. Acta*, 2001**, 84**, 3015. (b) K. S. Pillai, F. Krumeich, H.-J. Muhr, M. Niederberger, R. Nesper, *Solid State Ionics*, **2001**, *141-142*, 185. (c) M. E. Spahr, P. Bitterli, R. Nesper, M. Müller, F. Krumeich, H. U. Nissen, *Angew. Chem. Int. Ed.*, 1998, **37**, 1263.

[66] X. Chen, X. Sun, Y. Li, *Inorg. Chem.*, 2002, **41**, 4524.

[67] (a) G. T. Chandrappa, N. Steunou, S. Cassaignon, C. Bauvais, J. Livage, *Catal. Today*, 2003, **78**, 85. (b) G. T. Chandrappa, N. Steunou, S. Cassaignon, C. Bauvais, P. K. Biswas, J. Livage, *J. Sol-Gel Sci. Technol.*, 2003, **26**, 593.

[68] F. Krumeich, H.-J. Muhr, M. Niederberger, F. Bieri, R. Nesper, *Z. Anorg. Allg. Chem.*, 2000, **626**, 2208.

[69] (a) M. Wörle, F. Krumeich, F. Bieri, H.-J. Muhr, R. Nesper, *Z. Anorg. Allg. Chem.*, 2002, **628**, 2778. (b) V. Petkov, P. Y. Zavalij, S. Lutta, M. S. Whittingham, V. Parvanov, S. Shastri, *Phys. Rev. B.*, 2004, **69**, 085410-1.

[70] (a) M. E. Spahr, P. Stoschitzki-Bitterli, R. Nesper, O. Haas, P. Novak, *J. Electrochem. Soc.*, 1999, **146**, 2780 (b) S. Nordlinder, J. Lindgren, T. Gustafsson, K. Edström, *J. Electrochem. Soc.*, 2003, **150**, E280. (c) S. Nordlinder, A. Augustsson, T. Schmitt, J. Guo, L. C. Duda, J. Nordgren, T. Gustafsson, K. Edström, *Chem. Mater.*, 2003, **15**, 3227. (d) S. Nordlinder, L. Nyholm, T. Gustafsson, K. Edström, *Chem. Mater.*, 2006, **18**, 495. (e) A. Dobley, K. Ngala, S. Yang, P. Y. Zavalij, M. S. Whittingham, *Chem. Mater.*, 2001, **13**, 4382. (f) M. Malta, G. Louarn, N. Errien, R. M. Torresi, *J. Power Sources*, 2006, **156**, 533.

[71] (a) S. Webster, R. Czerw, R. Nesper, J. DiMaio, J.-F. Xu, J. Ballato, D. L. Carroll, *J. Nanosci. Nanotech.* 2004, **4**, 260. (b) J. Cao, J. Choi, J. L. Musfeldt, S. Lutta, M. S. Whittingham, *Chem. Mater.*, 2004, **16**, 731. (c) J. -F. Xu, R. Czerw, S. Webster, D. L. Carroll, J. Ballato, R. Nesper, *Appl. Phys. Lett.* 2002, **81**, 1711.

[72] (a) L. Krusin-Elbaum, D. M. Newns, H. Zeng, V. Derycke, J. Z. Sun, R. Sandstrom, *Nature*, 2004, **431**, 672; (b) E. Vavilova, I. Hellmann, V. Kataev, C. Täschner, B. Büchner, R. Klingeler, *Phys. Rev. B.*, 2006, **73**, 144417-1. (c) S. V. Demishev, A. L. Chernobrovkin, V. V. Glushkov, A. V. Grigorieva, E. A. Goodilin, H. Ohta, S. Okubo, M. Fujisawa, T. Sakurai, N. E. Sluchanko, N. A. Samarin, A. V. Semeno, *Phys. Rev. B.*, 2011, **84**, 094426-1.

[73] H. Nefzi, F. Sediri, *J. Solid State Chem*., 2013, **201**, 237.

[74] (a) B. Azambre, M. J. Hudson, *Mater. Lett.*, 2003, **57**, 3005. (b) B. Azambre, M. J. Hudson, O. Heintz, *J. Mater. Chem.*, 2003, **13**, 385.

[75] H. A. Therese, F. Rocker, A. Reiber, J. Li, M. Stepputat, G. Glasser, U. Kolb, W. Tremel, *Angew. Chem. Int. Ed.*, 2005, **44**, 262.

[76] C. O'Dwyer, D. Navas, V. Lavayen, E. Benavente, M. A. Santa Ana, G. Gonzalez, S. B. Newcomb, C. M. Sotomayor Torres, *Chem. Mater.*, 2006, **18**, 3016.

[77] W. Chen, J. Peng, L. Mai, Q. Zhu, Q. Xu, *Mater. Lett.*, 2004, **58**, 2275.

[78] L. I. Vera-Robles, A. Campero, *J. Phys. Chem. C*, 2008, **112**, 19930.

[79] H. Kweon, K. W. Lee, E. M. Lee, J. Park, I. -M. Kim, C. E. Lee, G. Jung, A. Gedanken, Y. Koltypin, *Phys. Rev. B*, 2007, **76**, 045434-1.

[80] D. Sun, C. W. Kwon, G. Baure, E. Richman, J. MacLean, B. Dunn, S. H. Tolbert, *Adv. Funct. Mater.*, 2004, **14**, 1197.

[81] S. H. Tolbert, C. C. Landry, G. D. Stucky, B. F. Chmelka, P. Norby, J. C. Hanson, A. Monnier, *Chem. Mater.*, 2001, **13**, 2247.

[82] J. N. Israelachvili, *Intermolecular and Surface Forces*, 2nd ed., Academic Press, London, 1992.

[83] M. Jaber, F. Ribot, L. Binet, V. Briois, S. Cassaignon, K. J. Rao, J. Livage, N. Steunou, *J. Phys. Chem. C*, 2012, **116**, 25126.

[84] G. T. Chandrappa, N. Steunou, J. Livage, *Nature*, 2002, **416**, 702 ; (b) O. Durupthy, M. Jaber, N. Steunou, J. Maquet, G. T. Chandrappa, J. Livage, *Chem. Mater.* 2005, **17**, 6395.

[85] L. Bouhedja, N. Steunou, J. Maquet, J. Livage, *J. Solid State Chem.*, 2001, **162**, 315.

[86] X. Rui, J. Zhu, W. Liu, H. Tan, D. Sim, C. Xu, H. Zhang, J. Ma, H. H. Hng, T. M. Lim, Q. Yan, *RSC Adv.*, 2011, **1**, 117.

[87] G. T. Kim, J. Muster, V. Krstic, J. G. Park, Y. W. Park, S. Roth, M. Burghard, *Appl. Phys. Lett.*, 2000, **76**, 1875.

[88] (a) L. Biette, F. Carn, M. Maugey, M. F. Achard, J. Maquet, N. Steunou, T. Livage, H. Serier, R. Backov, *Adv. Mater.*, 2005, **17**, 2970 ; (b) H. Serier, M.-F. Achard, O. Babot, N. Steunou, J. Maquet, J. Livage, C. M. Leroy, R. Backov, *Adv. Funct. Mater.*, 2006, 16, 1745; (c) C. M. Leroy, M. F. Achard, O. Babot, N. Steunou, P. Massé, J. Livage, L. Binet, N. Brun, R. Backov, *Chem.Mater.*, 2007, **19**, 3988; (d) J. Dexmer, C. M. Leroy, L. Binet, V. Heresanu, P. Launois, N. Steunou, C. Coulon, J. Maquet, N. Brun, J. Livage, R. Backov, *Chem. Mater.*, 2008, **20**, 5541.

[89] M. Li, G. Sun, P. Pin, C. Ruan, K. Ai, *ACS, Appl. Mater. Interfaces*, 2013, **5**, 11462.

[90] B. Yan, L. Liao, Y. You, X. Xu, Z. Zheng, Z. Shen, J. Ma, L. Tong, T. Yu, *Adv. Mater.*, 2009, **21**, 2436.

[91] G. Gu, M. Schmid, P.-W. Chiu, A Minett, J. Fraysse, G. -T. Kim, S. Roth, M. Kozlov, E. Munoz, R. H. Baughman, *Nature Mater.*, 2003, **2**, 316.

[92] R. Tenne, *Angew. Chem. Int. Ed.*, 2003, **42**, 5124.

[93] E. Uchaker, M. Gu, N. Zhou, Y. Li, C. Wang, G. Cao, *Small*, 2013, **9**, 3880.

[94] E. Uchaker, G. Cao, *Nano Today*, 2014, **9**, 499.

[95] (a) A. M. Cao, J. -S. Hu, H. -P. Liang, L. -J. Wan, *Angew. Chem. Int. Ed.*, 2005, **44**, 4391; (b) S. Wang, Z. Lu, D. Wang, C. Li, C. Chen, Y. Yin, *J. Mater. Chem.*, 2011, **21**, 6365; (c) M. Wu, X. Zhang, S. Gao, X. Cheng, Z. Rong, Y. Xu, H. Zhao, L. Huo, *CrystEngComm.*, 2013, **15**, 10123; (d) E. Uchaker, N. Zhou, Y. Li, G. Cao, *J. Phys. Chem. C*, 2013, **117**, 1621; (e) L. Mai, Q. An, Q. Wei, J. Fei, P. Zhang, X. Xu, Y. Zhao, M. Yan, W. Wen, L. Xu, *Small*, 2014, **10**, 3032.

[96] (a) M. R. Parida, C. Vijayan, C. S. Rout, C. S. Suchand Sandreep, R. Philip, P. C. Deshmukh, *J. Phys. Chem. C*, 2011, **115**, 112; (b) M. Zeng, H. Yin, K. Ye, *Chem. Eng J.*, 2012, 188, 64.

[97] L. Whittaker, J. M. Velazquez, S. Banerjee, *CrystEngComm.*, 2011, **13**, 5328.

[98] R. Levi, M. Bar-Sadan, A. Albu-Yaron, R. Popovitz-Biro, L. Houben, C. Shahar, A. Enyashin, G. Seifert, Y. Prior, R. Tenne, *J. Am. Chem. Soc.*, 2010, **132**, 11214.